AIAA JOURNAL
Vol. 45, No. 4, April 2007

Active Control of a Mach 0.9 Jet for Noise Mitigation Using Plasma Actuators

M. Samimy,* J.-H. Kim,† J. Kastner,‡ I. Adamovich,§ and Y. Utkin¶
The Ohio State University, Columbus, Ohio 43235-7531

DOI: 10.2514/1.27499

Localized arc filament plasma actuators were used to control an axisymmetric Mach 0.9 jet with a Reynolds number based on the nozzle exit diameter of 7.6×10^5. Eight actuators, distributed azimuthally inside the nozzle, near the nozzle exit, were used to excite various instabilities and azimuthal modes of the jet over a large Strouhal number range (St_{DF} of 0.1 to 5.0). Time-resolved pressure measurements were used to investigate the development of actuation perturbations in the jet, particle image velocimetry measurements were used to evaluate the control effects on the turbulence field, and far-field sound was measured to evaluate the control effects on the radiated acoustic field. The jet responded to the forcing over a large range of excitation Strouhal numbers with varying degrees. As expected, the low Strouhal number seeded disturbances grew slowly, saturated farther downstream, and stayed saturated for a longer time before decaying gradually. The saturation and decay of the seeded perturbations moved farther upstream as their Strouhal number was increased. Seeded perturbations with higher azimuthal modes exhibited faster decay. Particle image velocimetry results showed that when exciting the jet's preferred-mode instability at lower azimuthal modes, the jet potential core was shortened and the turbulent kinetic energy was increased significantly. At higher Strouhal numbers and higher azimuthal modes, forcing had less of an impact on the mean velocity and turbulent kinetic energy. Far-field acoustic results showed a significant noise increase (2 to 4 dB) when the jet is excited around the jet's preferred-mode instability Strouhal number ($St_{DF} = 0.2$–0.5), in agreement with the results in the literature. Noise reduction of 0.5 to over 1.0 dB is observed over a large excitation Strouhal number range; this reduction seems to peak around $St_{DF} = 1.5$ to 2.0 at a 30-deg angle, but around $St_{DF} = 3.0$ to 3.5 at a 90-deg angle. Although forcing the jet with higher azimuthal modes is advantageous for noise mitigation at a 30-deg angle and lower Strouhal numbers, the effect is not as clear at higher forcing Strouhal numbers and at a 90-deg angle.

Nomenclature

D	=	nozzle exit diameter
f_n	=	most amplified initial shear layer frequency
f_F	=	forcing frequency
f_p	=	jet's preferred-mode frequency
m	=	azimuthal mode number
p	=	pressure
St_D	=	Strouhal number based on the nozzle exit diameter, fD/U_j
St_{DF}	=	Strouhal number based on the forcing frequency, $f_F D/U_u$
St_θ	=	Strouhal number based on the boundary-layer momentum thickness at the nozzle exit, $f_0\theta_0/U_j$
U_j	=	nozzle exit velocity (jet centerline velocity within the potential core)
U_∞	=	freestream velocity
x	=	distance from the nozzle exit along the jet centerline
y	=	vertical distance from the jet centerline
θ_0	=	momentum thickness at the nozzle exit or at the trailing edge of the splitter plate
ρ	=	density
σ_u, σ_v	=	rms fluctuation of the x and y direction velocity

Presented as Paper 2703 at the 12th AIAA/CEAS Aeroacoustics Conference, Cambridge, MA, 8–10 May 2006; received 25 August 2006; revision received 14 December 2006; accepted for publication 3 January 2007.

*Professor, Director of Gas Dynamics and Turbulence Laboratory, Department of Mechanical Engineering, 2300 West Case Road. Associate Fellow AIAA.

†Research Associate, Gas Dynamics and Turbulence Laboratory, Department of Mechanical Engineering, 2300 West Case Road. Member AIAA.

‡Graduate Student, Gas Dynamics and Turbulence Laboratory, Department of Mechanical Engineering, 2300 West Case Road. Student Member AIAA.

§Associate Professor, Nonequilibrium Thermodynamics Laboratory, Department of Mechanical Engineering, 201 West 19th Avenue. Associate Member AIAA.

¶Postdoctoral Researcher, Nonequilibrium Thermodynamics Laboratory, Department of Mechanical Engineering, 201 West 19th Avenue. Member AIAA.

I. Introduction

PLANAR free shear or mixing layers have received tremendous attention over the past several decades, because these canonical flows are the building blocks in many practical applications. The discovery of large-scale coherent structures in high Reynolds number free shear flows by Brown and Roshko [1] and the realization that these structures play a major role in entrainment and bulk mixing [2] and in far-field radiated noise production [3] has changed the nature of the research over the past three decades by putting more focus on the dynamics and control of these structures. A review article by Ho and Huerre [4] details most of the early work on the physics of low-speed free shear flows, as well as their control, over about two decades. A review article by Tam [5] details the work in jet noise and the role of large-scale structures.

A. Instability of Free Shear Layers and Axisymmetric Jets

A planar free shear layer is known to be unstable and acts like an amplifier of disturbances in the flow over a range of frequencies. The instability of free shear layers is referred to as Kelvin–Helmholtz (K–H) instability. In sufficiently high Reynolds numbers, the effect of viscosity in the amplification of disturbances is relatively small, and thus the instability is also called inviscid instability. Detailed linear stability analysis [6,7] over the years has shown that the most amplified Strouhal number scales with the momentum thickness of the boundary layer at the trailing edge of the splitter plate ($St_\theta = f_n\theta_0/U_\infty \sim 0.013$). Subsequent experimental investigations

have not only confirmed the existence of such an instability mechanism and the scaling of St_θ with θ_0, but have also shown that the initial waves due to the K–H instability mechanism roll up into large-scale structures [1,4]. These structures entrain the fluid into the mixing layer from both sides and play a major role in the bulk mixing of the fluids [2]. Also, their dynamics are generally believed to be responsible for a significant portion of the far-field radiated noise.

In a planar free shear layer without any seeded disturbances, natural disturbances exist but are random in nature, and as a result, the vortex roll-up and subsequent merging processes are also random. Therefore, large-scale structures are not often spatially or temporally coherent, and merging locations are not spatially fixed. By the introduction of a low-amplitude forcing, the events could be manipulated and changed dramatically and could be made much more organized [2,4,8]. In a forced shear layer, the processes of vortex roll-up and subsequent merging takes place in an organized fashion.

Over the years, numerous researchers have investigated and played a role in shedding light on the physics of axisymmetric jets, owing to their many engineering applications, in addition to scientific curiosity. Axisymmetric jets add two more complexities to the planar shear layers. The first one arises from azimuthal modes in the axisymmetric shear layer, which compete for energy and grow selectively. The second one arises from the inward growth of the free shear layer toward the jet axis and its eventual interaction around the centerline, which ends the jet potential core.

The ratio of the nozzle exit diameter to the boundary-layer momentum thickness at the nozzle exit (D/θ_0) seems to be the principal factor in deciding which of the azimuthal modes would grow. Linear stability analysis [6,7,9] and experimental work [10–12] have shown that for large D/θ_0 ($D/\theta_0 \gg 1$), both axisymmetric ($m = 0$) and the first helical modes ($m = \pm 1$ or -1) are unstable in the initial jet shear layer. Linear stability analysis [10] also showed that for a very thin boundary layer (or very large D/θ_0), many azimuthal modes are unstable in the initial shear layer region. Linear stability analysis [7] also showed that farther downstream in the jet, where the velocity profile has gradually changed from being top-hat-shaped to bell-shaped, the jet can only support helical modes. It has also been reported that the growth region of helical modes moves farther upstream toward the nozzle as the jet velocity increases [4].

In an axisymmetric jet, the inward growth of the jet shear layer and its interaction around the jet axis ends the typical merging of successive large-scale structures and starts an additional interaction: azimuthal interaction. The average location at which the jet centerline velocity begins to decay is called the end of jet potential core. This interaction, which is dynamic and nonlinear, adds tremendous complexity to the problem. Standard linear stability analysis, which has been a guiding light in the understanding of free shear layers and is applicable only in the early development of the shear layer up to roll-up, is no longer helpful.

Many researchers have shown experimentally that the passage Strouhal number of large-scale structures at the end of potential core, called the jet preferred mode or jet column mode Strouhal number, is scaled with the nozzle exit diameter, $St_D = f_p D/U_u \sim 0.2$ to 0.6 [13–16]. Although the St_D seems to vary over a large range, it is often close to 0.3 [4]. The variations stem from two main sources [17]. The first one is nonphysical and related to where in the jet and how St_D is measured. The second one is physical and related to the dominant disturbances in a given facility. The pseudononlinear stability analysis of Crighton and Gaster [18] puts this mode at $St_D = 0.4$.

If merging of large-scale structures takes place sequentially, it is relatively obvious that the jet's preferred-mode frequency would be related to the most amplified shear-layer-mode frequency by $f_n/f_p = 2^n$, where n is the number of pairings taken place before the end of potential core. This proportionality seems to hold in low-speed flows with large boundary-layer momentum thickness, but f_p locks onto a fixed frequency at higher velocities [4]. The reason for this locking is not clear. Hussain and Zaman [16] reported that in jets forced at the preferred-mode frequency, the structures lock onto this frequency by two to three nozzle diameters downstream and there is no tendency for pairing or subharmonic growth. It is not clear in the literature how we get from the most amplified mode (or structure) frequency to the preferred-mode (structure) frequency in axisymmetric jets. One can think of two potential routes. The first is the typical growth and roll-up of the most amplified mode and then sequential pairing, as is known to occur in planar shear layers. The second potential process could involve "collective interaction," also seen in planar shear layers [2,8], in which more than a pair of vortices interact and merge. This collective interaction has also been proposed by others [19,20] as a "source of order" in shear layers. It is also possible that the mechanism for this process does not fit into the standard form of vortex interactions.

B. Control of Axisymmetric Jets for Noise Mitigation

Flow control is divided into two general categories: passive and active. Passive control does not add energy to the flow and is often accomplished by geometric modifications. In active control, energy is added to the flow to excite flow instabilities or affect the flow by way of generating new flow structures (e.g., streamwise vortices). Active control is further divided into open loop and closed loop. In the open-loop control, actuations take place based on an operator's command or a predetermined input. In the closed-loop control, information from a sensor or sensors in the flow, along with a flow model, guides the actuation process [21]. Only passive control and active open-loop control will briefly be discussed next.

There has been a surge in the passive control of jets in recent years, primarily motivated by noise mitigation. Passive control of jets and mixing layers is accomplished via geometrical modifications of the nozzle trailing edge using tabs, chevrons, and lobbed nozzles [22–28]. Tabs generate pairs of streamwise vortices in the jet [23] and provide a reduction in the far-field overall sound pressure level (OASPL) [29–31]. A drawback of tabs is that they protrude into the jet and thus provide a thrust loss. For this reason, devices like chevrons, which have significantly less area blockage than tabs, are presently implemented into full-scale aircraft engines for noise mitigation.

Open-loop active control can be divided into two categories. The first category involves steady or low-frequency (a frequency that is much lower than any instability frequency in the flow) energy addition to the flow. A few examples include steady fluidic injection through microjets [32,33] and fluidic chevrons [34]. These are considered active control due to the energy addition, but they do not have frequency or phase control, which is essential when exciting flow instabilities. The second category involves using actuators with frequency capabilities in the range of flow instability frequencies. This is the subject of the current work and will be further discussed next.

The majority of the investigations using open-loop control have been carried out in relatively low-speed and low Reynolds number jets. The upper edge of the Reynolds number based on jet diameter seems to be around 50,000 for the majority of these works [35]. As the speed and the Reynolds number of the jet increase, so do the background noise, the instability frequencies, and the flow momentum. Therefore, actuators must provide excitation signals of much higher amplitude and frequencies: two diametrically opposing requirements. As a result, there is only a limited number of works in the active control of high-speed and high Reynolds number jets. Several researchers [3,36–39] used acoustic forcing (either by channeling the acoustic signal to multiple locations at the proximity of the nozzle exit or by placing the acoustic driver in the jet settling chamber) to force a high subsonic jet around its preferred mode with some success. Kibens et al. [40] used high-amplitude pulsed injection to control the jet exhausting from a full-scale jet engine at the flapping mode ($m = \pm 1$). The increased scale (and thus the reduced frequency) was a key factor in the implementation of actuation in this work. A few investigations have also been carried out in high-speed jets but low Reynolds number [41,42].

Work involving jet and shear layer control using acoustic drivers has helped in revealing some of the characteristics of flow instabilities and their relation to the far-field sound. For example, when forcing the jet around the jet column instability, the broadband

noise is amplified and a high-amplitude tone appears at the forcing Strouhal number in the far-field [3,25,37]. Along with the increase in the far-field noise, there is an increase of turbulence intensity in the flowfield [39]. The broadband amplification has also been shown for jets with coflow [38] and for heated jets [36]. When forcing the various azimuthal modes m of the jet around the jet column instability Strouhal number, the broadband is still amplified, but the radiated tones are weaker in amplitude [43]. The acoustic field for jets forced at higher than the jet's preferred-mode Strouhal number has also been investigated. Moore [3] showed a slight reduction in broadband noise for $St_D > 1.5$ and Mach number less than 0.8. A major limitation in these works was the limits imposed by the actuators' frequency and amplitude. As already stated, it is difficult to excite high Reynolds number jets, which require higher-amplitude and higher-frequency actuation.

We have recently developed a class of plasma actuators, called localized arc filament plasma actuators (LAFPA) that can provide excitation signals of high amplitude and high bandwidth for high-speed, high Reynolds number flow control [44–48]. The actuators' frequency, phase, and duty cycle (the percentage of time an actuator is on in a cycle for a given frequency) can be controlled independently. Therefore, several of these actuators can be used to force the jet column instability, shear layer instability, and various azimuthal modes. In the following sections, we will first provide a brief background on plasma-based actuators in general, then on LAFPA in particular.

C. Plasma-Based Actuators for Flow Control

In recent years, there has been a considerable interest in the use of electric discharge plasmas for flow control (a more detailed overview can be found in [47,48] and references therein). The primary mechanisms of plasma flow control include electrohydrodynamic (EHD) interaction [49,50], magnetohydrodynamic (MHD) interaction [51,52], and thermal methods [53–57]. The limitation on the use of EHD flow control is the necessity to generate significant ion density in the space charge region of electric discharge (i.e., cathode sheath or streamer head). Although EHD plasma actuators can be quite energy-efficient, their use for high-speed flow control (with flow velocities of a few hundred meters per second at near atmospheric pressure) does not appear feasible at the present time. Similarly, for the MHD flow control, the limitation is the necessity to sustain significant flow conductivity, except for high-temperature hypersonic reentry flows. Sustaining high conductivity using nonequilibrium plasmas is limited by ionization instabilities and requires a prohibitively high plasma power budget.

Recent work by Leonov et al. [55] indicated that a significant high-speed flow control potential could be realized using the thermal effect of near-surface, high-current, high-temperature arc discharges. It was shown that the intense, localized, rapid heating produced by plasmas in high-current electric discharges may produce shock waves and considerably modify the supersonic flow. Basically, rapid near-adiabatic heating results in an abrupt pressure jump in the current filament, which suggests that rapidly heated regions located near surfaces could be used to force various instabilities in free shear layers and jets. The proximity of the pulsed arc plasma to the wall greatly improves its stability and reduces the chance of plasma being blown off by the incident high-speed flow. However, the most crucial aspect of the effect of repetitively pulsed arc plasmas on the flowfield (specifically, producing local disturbances of high amplitude and high frequency to control flow instabilities) remained uncharted until the recent work by our group [44–48]. Note that the nature of a high-temperature, localized arc discharge is completely different from low-temperature, low-current, diffuse glow discharges used in previous low-speed flow control work [49,50]. The fundamental difference is that in the present approach, the flow is affected by localized perturbations produced by arc-generated localized pressure and temperature spikes (which are purely thermal effects), whereas low-speed glow discharge flow control relies on nonthermal EHD interaction between diffuse plasma and the flow.

The experimental facility and techniques used in the current research will be described in the following section. The presentation will include flow facility, flow and acoustic diagnostic techniques, and the plasma actuators, including their power supply and control system.

II. Experimental Facility and Techniques

A. Flow Facility

All of the experiments were conducted in the Gas Dynamics and Turbulence Laboratory at The Ohio State University. The ambient air is compressed, dried, and stored in two cylindrical tanks at a pressure of up to 16 MPa with a capacity of 36 m^3. The compressed air is supplied to the stagnation chamber and conditioned before entering into a nozzle. An axisymmetric converging nozzle, which was operated at Mach 0.9, was used. The air is discharged horizontally through the nozzle into an anechoic chamber (Fig. 1). The exit diameter of the nozzle is 2.54 cm (1.0 in.). A nozzle extension, made of boron nitride, was attached to the exit of the nozzle to house the plasma actuators. The facility is designed to accommodate laser-based flow diagnostics in a fully anechoic environment. The inner dimensions of the chamber, from wedge tip to wedge tip, are 3.1 m in width and length, and 2.7 m in height. Additional details of the anechoic chamber, its validation, and the jet facility can be found in [31].

The Reynolds number of the jet based on the jet diameter was 7.6×10^5 for the Mach 0.9 jet. The boundary-layer thickness at the exit of the nozzle is very thin, making it impossible to obtain a boundary-layer profile to determine its momentum thickness and its state. Kastner et al. [58] used a similar converging nozzle and measured a few points within the boundary layer of a Mach 0.9 jet. They estimated the boundary layer to be turbulent, with a thickness of about 1 mm and a momentum thickness of about 0.1 mm. The characteristics of the boundary layer in the current experiments are expected to be quite similar.

B. Flow and Acoustic Diagnostic Techniques

Two-component particle image velocimetry (PIV) was used to measure the x and y components of velocity on the illuminated x–y plane (Fig. 1). Images were acquired and processed using a LaVision PIV system with a 2000 by 2000 pixel Redlake CCD camera employing a 75–300-mm Vivitar zoom lens with a 532-nm narrowband optical filter. Other essential hardware and software are housed in a dedicated computer with dual Intel Xeon processors. The system triggers a dual-head Spectra Physics PIV-400 Nd:YAG laser operating at the 2nd harmonic (532 nm). Each laser head was operated at an approximately 350-mJ-per-pulse energy level for PIV measurements. Image pairs were acquired at a sampling rate of approximately 5 Hz.

The jet was seeded with di-ethyl-hexyl-sebacat fluid introduced 2.75 m upstream of the nozzle exit by a four-jet atomizer. This location was chosen to provide homogenous dispersion of the seed particles throughout the jet. A free jet entrains a significant amount of ambient air. For this reason, a portion of the ambient was seeded by

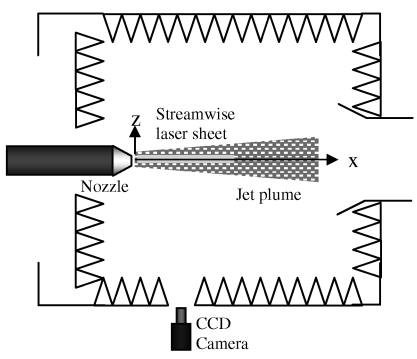

Fig. 1 Schematic of the jet and the PIV setup; the y coordinate is normal to the plane (not to scale).

injecting fog from a fog generator into a 15-in.-diam cylinder located symmetrically around the jet. A small amount of air was also injected into the cylinder to generate a very low-speed coflow. The camera views the streamwise laser sheet orthogonally over the first 9 to 10 jet diameters. The time separation between laser pulses was 2.0 μs. The PIV images were divided into 32 by 32 pixel interrogation windows. Subregions for each image pair were cross-correlated using multipass processing with a 50% overlap to improve the spatial resolution and prevent the appearance of spurious vectors by adaptively improving the window size. Initial passes used 64 by 64 pixel interrogation windows that were then used as a reference for the 32 by 32 pixel windows in the final pass. This experimental setup produced a velocity vector grid of 115 by 65 over the measurement domain. This translated to each velocity vector being separated by approximately 2 mm. To calculate turbulence statistics, 700 PIV images were used.

A Kulite pressure transducer probe was used to measure the growth and decay of the seeded perturbations by the plasma actuators. The axis of the probe was normal to the jet axis so that real-time static pressure, rather than total pressure, was measured. The probe tip was located at the lip line of the nozzle radially, at the center of actuator 7 azimuthally (Fig. 2), and traversed in the streamwise direction manually from $x/D = 0.5$ to 7.5. The signal from the probe was amplified, low-pass filtered and then sampled at 200 kHz per channel by a National Instruments A/D board. The window size was 8192 points, providing a frequency resolution of 24.4 Hz. An average spectrum was obtained from 100 short-time spectra for each case, and the perturbation level at the forcing Strouhal number was calculated from the average spectrum. For the baseline case, the level was obtained at a Strouhal number matching the specific forcing Strouhal number. The perturbation level was normalized by 2×10^{-5} Pa in all cases. It should be noted that this is not an accurate real-time static pressure measurement technique, but an approximate way of exploring the development of seeded perturbations into the flow.

Far-field sound pressure level (SPL) was measured using two 1/4-in. B&K microphones, located 30 and 90 deg relative to the jet axis, 83 and 45D from the nozzle exit, respectively. The far-field acoustic results were normalized to a radius of 80D. The acoustic signal from each microphone was conditioned, bandpass filtered from 20 to 100 kHz, and amplified by a four-channel B&K Nexus conditioning amplifier. The microphones were calibrated using a 94-dB, 1-kHz sine wave, and the frequency response of the microphone was flat up to 80 kHz when the microphone grid cover was removed. The sampling parameters were the same as in the Kulite signal acquisition and data processing, and an average spectrum was obtained from 100 short-time spectra.

As will be discussed next, pulsed arc filament discharges produced by the plasma actuators generate electromagnetic interference (EMI) that could contaminate acoustic signals. The microphones were muffled and noise was measured to check for any sign of signal contamination. The muffled spectrum did not show any tones at the forcing frequency and thus the measured far-field acoustic was free of EMI contamination. A similar procedure was also used to check the potential EMI contamination of the measurements with Kulite pressure transducers.

C. Plasma Actuators and Plasma Generator System

Each actuator consists of a pair of pin electrodes. The electrodes are distributed around the nozzle perimeter (Fig. 2), approximately 1 mm upstream of the nozzle exit plane. A ring groove 0.5-mm deep and 1-mm wide was used to house the electrodes and to shield and stabilize the plasma. In our earlier experiments, the plasma was swept downstream by the flow without such a groove [44]. We have used various nozzle extensions attached to the nozzle exit to house the electrodes, as well as various type and size electrodes [44]. For the work presented here, the nozzle extension was made of boron nitride, and steel or tungsten wires of 1-mm diameter were used for electrodes. Tungsten wires have proved to be more resistant to the erosion caused by the arc discharge. Measured center to center, the spacing between a pair of electrodes for each actuator is 3 mm, and the eight actuators were uniformly distributed around the nozzle exit (Fig. 2).

Figure 2 shows a schematic of the multichannel high-voltage plasma generator, designed and built in-house. The plasma generator enables simultaneous powering of up to eight plasma actuators distributed around the perimeter of the ceramic nozzle extension, with independent frequency, duty cycle, and phase control of individual actuators. Each actuator is connected in series with a fast-response, high-repetition-rate, high-voltage MOSFET switch; two approximately 15-kΩ high-power solid body ceramic ballast resistors; and a high-voltage, high-current (10 kV, 1 A) dc power supply (Glassman High Voltage, Inc.). Two of these power supplies are used to energize eight actuators. If all eight actuators are powered at the same time, the single actuator current is limited to 0.25 A. The switches are controlled by using an eight-channel digital-to-analog output PCI card and LabView software, which allows their independent frequency, duty cycle, and phase control. The switches are capable of producing high-voltage pulses (up to 10 kV) at repetition rates from 0 to 200 kHz, with a very short pulse rise/fall time ($\sim$0.1 μs) and a variable duty cycle (from 0 to 100%). Every switch is liquid-cooled to allow continuous operation at high frequency, voltage, and current.

By turning the electronic switch on and off, positive high-voltage pulses can be applied to the corresponding actuator. The high initial voltage is needed to produce breakdown in the approximately atmospheric pressure air in the gap between the two electrodes of an actuator, which are 3 mm apart in the present work. After the breakdown, the arc is generated and the voltage across the gap rapidly falls to a few hundred volts. The plasma generator is compact,

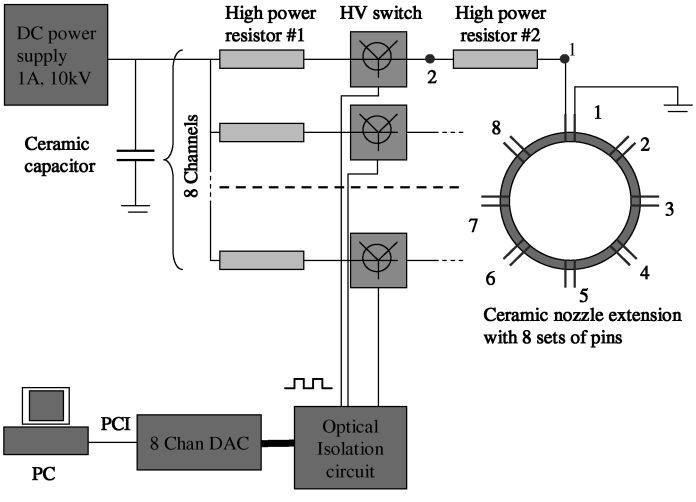

Fig. 2 Schematic of the in-house fabricated plasma generator.

robust, and simple to operate. In the present work, continuous operation of all eight actuators in a Mach 0.9 jet (up to several minutes) has been achieved. To reduce the EMI interference with the computer and data acquisition board, an in-house-built optical isolation circuit was implemented in the low-voltage side.

In a typical acoustic driver, which has been used extensively in the literature for flow control, the input signal is a sine wave of prescribed frequency and peak amplitude. The input amplitude changes gradually between the given positive and negative peaks in a cycle. On the other hand, the input signal to a plasma actuator is a rectangular wave with a variable duty cycle (for more details, see [47,58]). In a plasma actuator, the input or forcing amplitude cannot easily be altered, as in an acoustic driver. Although the imparted forcing energy to the flow in a cycle can be adjusted by adjusting duty cycle, the effective forcing amplitude is not directly related to the total energy in a cycle. However, it is straightforward to force the jet in any simple azimuthal mode ($m = 0, 1, 2, 3, \ldots, N/2 - 1$; N being the number of actuators used), because there is no forcing amplitude variation. For combined/mixed azimuthal modes ($m = \pm 1, \pm 2, \ldots$), the input amplitude is the modulated amplitudes of the positive and negative waves. These modes were simulated or mimicked by grouping the actuators without any amplitude modulation, which is not possible with the plasma actuators. For example, the top three actuators (1, 2, and 8) and the bottom three actuators (4–6) in Fig. 2 were grouped together and operated 180 deg out of phase to simulate the $m = \pm 1$ mode. For this mode, actuators 3 and 7 were not operated to make these positions nodal points of the $m = \pm 1$ mode. For other mixed modes, a similar grouping was done. There are two additional secondary effects specific to these plasma actuators. First, the actuator input signal has a prescribed frequency, but because it is a rectangular wave, it contains higher frequencies as well. Second, each actuator might generate a pair of very weak streamwise vortices. Although we plan to explore the second issue in the near future, any potential effects of the first subject, perceived to be small, are difficult to estimate.

III. Experimental Results and Discussions

Experimental results will be presented in this section. The results will be presented and discussed in the following order: characterization of plasma actuator input, development of actuation perturbation and the instability waves, flow visualization, and PIV and far-field acoustic results.

A. Plasma Actuator Input Characterization

Figure 3 shows, top to bottom, the time-dependent input signal to one of the plasma actuators (input signal to the high-voltage switch) and voltage, current, and power in the arc discharge between the two steel wire electrodes of the actuator, respectively. During these measurements, only one actuator was operated at 20-kHz frequency and a 20% duty cycle in an ideally expanded Mach 1.3 jet. Duty cycle refers to the percentage of time in a cycle that the input voltage is high or the actuator is turned on. Results in the Mach 0.9 jet are similar. The static pressure at the actuator's location (1 mm before the nozzle extension exit) was approximately 1 atm. The time-dependent voltage between the actuator electrodes was measured at station 1 (see Fig. 2) by a Tektronix high-voltage probe P6015A. A very large voltage spike (about 4.0 kV) at the onset of the cycle ($t \sim 15$ μs on the graph) corresponds to electrical breakdown in the air between the electrodes, followed by a sharp voltage drop to about 500 V as a stationary arc discharge is formed. After the discharge current is interrupted by rapidly closing the switch (10 μs later), the plasma is quickly blown off by the flow. As a result, the high-voltage electrode (anode) becomes floating and the voltage remains essentially unchanged (at about 500 V) until the moment the switch is opened again, 50 μs later.

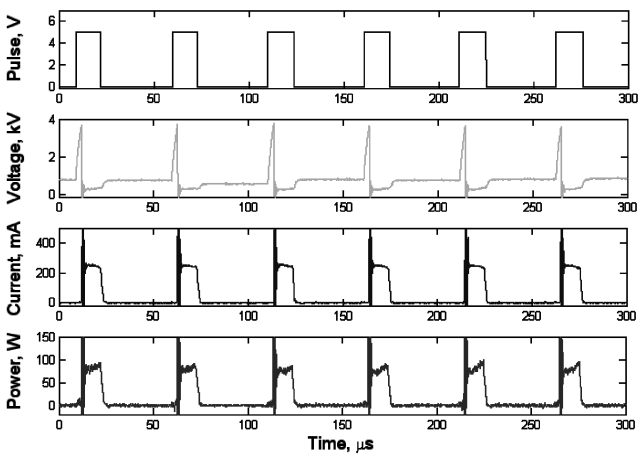

Fig. 3 Top to bottom, respectively, time-dependent input signal to the high-voltage switch; voltage, current, and power in a plasma actuator operated at 20-kHz frequency and 20% duty cycle (only one actuator was operated).

The actuator current was measured simultaneously with the voltage measurement using a LeCroy CP031 current probe. The current trace is nearly a step function, with the steady-state current of about 0.25 A when the switch is open and with no current when it is closed. The time-dependent arc discharge power is obtained simply by multiplying the current and voltage traces. The power during the current pulse reaches approximately 150 W, which corresponds to a time-averaged actuator power of only 30 W (i.e., 240-W net power for all eight actuators in operation). For comparison, the flow power (the total enthalpy flux) of the jet at these conditions is about 28 kW. These results demonstrate that high-speed flow control by localized arc plasma actuators can be highly energy-efficient. Note that the power generated by the dc power supply used to run the plasma actuators is significantly higher, with more than 90% of the power dissipating on the ballast resistors. However, the use of a more efficient power supply that produces a periodic, low-voltage, rectangular-shaped waveform with short high-voltage pulses to achieve breakdown at the beginning of each period would greatly reduce the power budget of the entire flow control system.

The measurements also showed that the voltage, current, and power traces for all eight actuators are essentially the same, except for the expected phase shifts in excitation of nonaxisymmetric modes. Depending on the frequency, mode, and duty cycle, the arc discharges produced by different actuators may overlap in time.

B. Growth and Decay of Perturbations and the Ensuing Instability Waves

A dynamic Kulite pressure transducer, located at the tip of a conical-cylindrical probe, was used to measure real-time pressure in the Mach 0.9 jet to explore the growth and decay of the perturbation seeded into the flow by plasma actuators and the instability waves. The transducer, located at the same azimuthal location as actuator number 7 in Fig. 2, was traversed in the streamwise direction from $x/D = 0.5$ to 7.5. The tip of the transducer grazes the shear layer at the first measurement location ($x/D = 0.5$), measuring real-time static rather than stagnation pressure, but is well into the shear layer in farther downstream locations, because the shear layer is growing. The amplitude of the local pressure at the forcing frequency was obtained using a power spectrum of the time-resolved Kulite pressure signal. As was mentioned earlier, this is not a precise measurement, but is sufficient for exploring the development of disturbances seeded by the actuators.

Figure 4 depicts the streamwise spatial development of the seeded perturbations at several Strouhal numbers when only actuator number 7 is operating and all of the other seven actuators are off. Essentially, the jet is perturbed locally in this case and is expected to respond locally. As the forcing Strouhal number increases from 0.18, two expected trends are observed. First, the saturation or the peak amplification location for the perturbation moves upstream. For example, the saturation locations for the forcing at St_{DF} of 0.18 and 0.63 are about $x/D = 4.0$ and 2.0, respectively. Second, the perturbation remains saturated (or the energy exchange with the

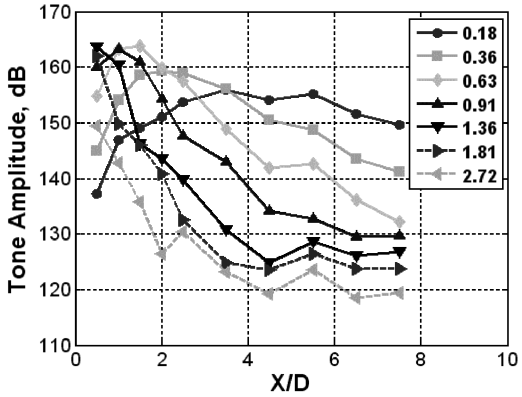

Fig. 4 Spatial development of seeded perturbations by one plasma actuator (no. 7) at several Strouhal numbers (St_{DF}).

mean flow is almost frozen) before decaying, for a longer distance at lower St_{DF} (e.g., about $4x/D$ for St_{DF} of 0.18 vs $0.5x/D$ for St_D of 0.63). At much higher St_{DF} (e.g., St_{DF} of 1.81 and 2.72), the growth and saturation have taken place before the first measurement location at x/D of 0.5, and the exchange of energy is from the perturbation to the mean flow over the entire measurement location.

Figure 5 shows the spatial development of the seeded perturbations/instability waves at four different Strouhal numbers when the jet is forced at various azimuthal modes ($m = 0$, 1, 2, and 3). For comparison, the results for the single actuator case (as was shown in Fig. 4) and the baseline case are also shown. Note that there is no external perturbation in the baseline case, but there are always natural and random disturbances in the flow. The trend is gradual growth to saturation, gradual decay at lower St_{DF}, and rapid growth and decay at higher St_{DF}. For the various azimuthal forcing cases, some interesting observations can be made. For example, around the preferred-mode Strouhal number forcing ($St_{DF} = 0.36$), the axisymmetric mode ($m = 0$) grows faster, reaching higher amplitude than the first helical mode ($m = 1$), but also decays faster. But this is not the case at higher Strouhal number forcing ($St_{DF} = 1.81$), where the $m = 0$ mode remains at a higher level than others for a much longer downstream distance. The energy exchange between various azimuthal modes and the mean flow seems to be similar in the instability wave/seeded perturbation growth phase, but significantly different in the decay phase: the higher azimuthal modes decay faster. For the forcing at $St_{DF} = 1.81$, the initial amplitudes for the various azimuthal mode excitation are similar, indicating no (or relatively mild) response of the jet to forcing at this Strouhal number. This is consistent with the flow results, which will be discussed in Sec. III.C. We were limited to $m = 3$ with the current eight-actuator arrangement. We will use more actuators, enabling us to force higher azimuthal modes, in the near future.

Figure 6 shows spatial development of the seeded perturbation/instability waves in the streamwise direction for the excitation of mixed azimuthal modes ($m = \pm1$, ±2, and ±4) at two St_{DF} of 0.36 and 0.91. The trends are similar to those of excitation of simple azimuthal modes. For the $m = \pm1$ mode, which is also called the flapping mode, the results are shown on the actuation/flapping plane (FP) and the nonflapping plane (NFP). The amplitude of the perturbation is much higher on the flapping plane, as expected. As in the simple azimuthal modes excitation cases, the higher modes contain much lower energy, especially in the lower forcing Strouhal number cases.

C. Flow Results

Planar flow visualization provides a great means, though qualitative, of exploring the effects of control on the flow structures. Visualizing flow structures in mixing layers and jets is best accomplished using product formation, which visualizes only the mixing region and reveals the complete cross section of large-scale structures. For a supersonic unheated jet, product formation occurs naturally as the cold and dry jet air mixes with the warmer and humid ambient air. Even though the focus of this paper is on a Mach 0.9 jet, Fig. 7, which is for an ideally expanded Mach 1.3 jet, is used here to visually illustrate the effect of forcing using plasma actuators. The exit diameter for this nozzle is also 2.54 cm (1.0 in.), and the Reynolds number of the jet based on the jet diameter is about 1.1×10^6. The nozzle exit boundary-layer conditions, the jet column

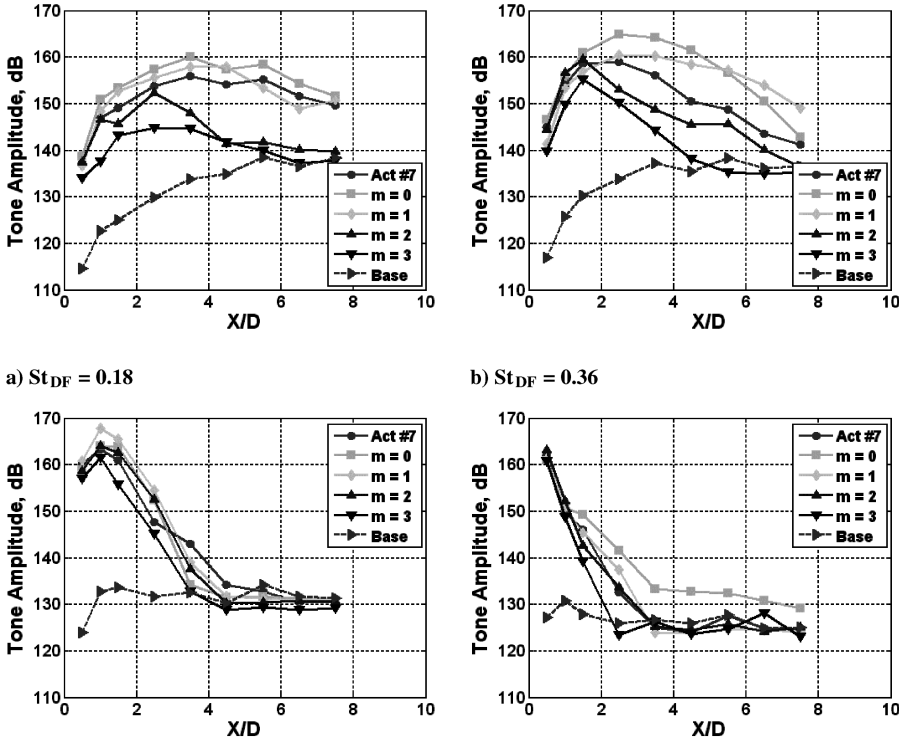

Fig. 5 Spatial development of seeded perturbations at four excitation Strouhal numbers for different azimuthal modes ($m = 0$–3).

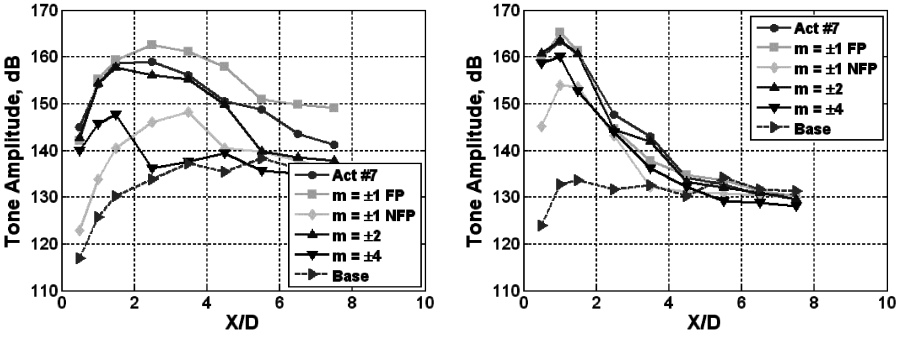

a) $St_{DF} = 0.36$ b) $St_{DF} = 0.91$

Fig. 6 Spatial development of seeded perturbations at two Strouhal numbers for forcing different mixed azimuthal modes ($m = \pm 1$, ± 2, and ± 4).

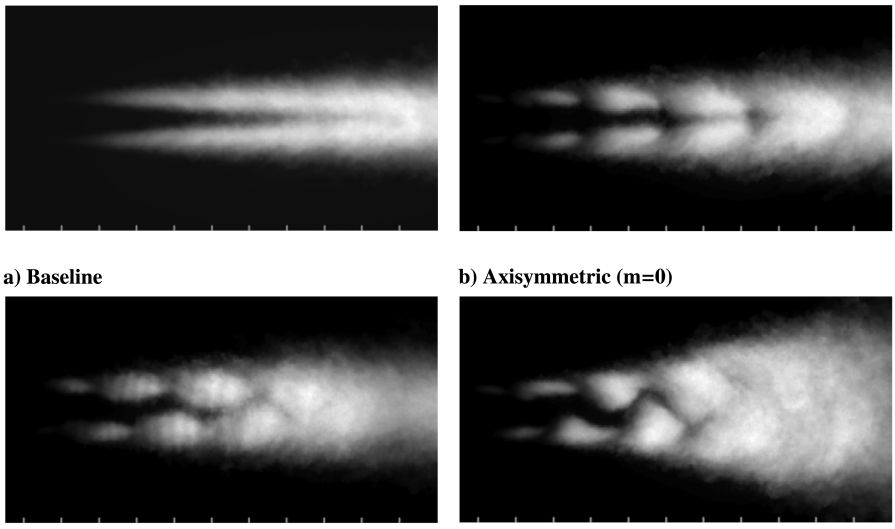

a) Baseline b) Axisymmetric (m=0)

c) First helical (m=1) d) Flapping (m = ±1)

Fig. 7 Average planar images of a Mach 1.3 ideally expanded axisymmetric jet: a) ensemble-averaged baseline jet, b)–d) phase-averaged jet forced with various azimuthal modes at $St_{DF} = 0.33$.

Strouhal number, and the most amplified Strouhal numbers are all similar in both jets. The location of the laser sheet and camera were similar to those in the PIV setup shown in Fig. 1. The distance between the two adjacent tick marks in the figure is one nozzle exit diameter and the first tick mark is at $1D$ from the nozzle exit. Figure 7a shows an ensemble-averaged image (based on 50 instantaneous images of 9-ns exposure time) of the baseline jet, which does not show, as expected, any large-scale structures. Figures 7b–7d show phase-averaged images of the jet forced with various azimuthal modes at $St_{DF} = 0.33$, which is around the jet-preferred Strouhal number [46,47]. Large-scale coherent structures are generated by the excitation, which are very well organized and robust, similar to large-scale coherent structures in low-speed and lower Reynolds numbers [1]. Also, the jet spread is significantly increased when it was forced in the flapping mode ($m = \pm 1$). The effect of forcing is expected to be very similar for the Mach 0.9 jet. Detailed results for the Mach 1.3 jet are given in [46,47].

The flow visualization results presented here are quite informative in helping to assess flow control effects. They could also provide some quantitative data such as wavelength and convective velocity of the structures [47]. To provide more quantitative data, we have used PIV measurements that we will now present and discuss.

PIV measurements have been obtained for a Mach 0.9 jet in the excitation Strouhal number range of $St_{DF} = 0.09$ to 3.08. Figure 8 shows the jet centerline velocity for the baseline case and forcing the $m = 1$ mode at several St_{DF}. As was shown earlier, forcing affects the jet over a large excitation Strouhal number range, but the effect is strongest from $St_{DF} = 0.18$ to 0.36 (around the jet-preferred St_D). Also, the excitation effect is negligible beyond approximately excitation St_{DF} of 1.81. As was discussed earlier, the excitation provides local heating right before the nozzle exit and the effects are observed only within the shear layer, which is very thin in the early stage of the development.

Therefore, there is no forcing effect at the jet centerline until past about four jet diameters downstream of the nozzle exit, where large-scale structures in the shear layer have grown sufficiently large to reach the jet centerline. A drastically reduced jet potential core and increased decay rate of the centerline Mach number of the jet beyond the end of potential core can be observed for forcing at both St_{DF} of 0.18 to 0.36, an indication of substantial mixing enhancement that was also observed in the flow visualization results for Mach 1.3 and the perturbation/instability wave development results in Fig. 5. The jet's preferred-mode Strouhal number for Mach 1.3 was about 0.33 [46,47]. Although it is slightly different for different azimuthal modes for Mach 0.9, from the results shown in Fig. 8, it appears to be somewhere between $St_D = 0.18$ and 0.36. At a much higher forcing Strouhal number, there do not seem to be any changes in the potential core length or the decay rate beyond the end of potential core. For example, the results for excitation at St_{DF} of 1.81 and 3.08 fall on top of the baseline case, indicating no excitation effect beyond about forcing St_{DF} of 1.81. The estimated Strouhal number based on the initial shear layer or the incoming boundary-layer momentum thickness St_θ for forcing at $St_{DF} = 1.81$ and 3.08 are about 0.007 and 0.012. The latter case is close to the estimated most amplified St_θ of

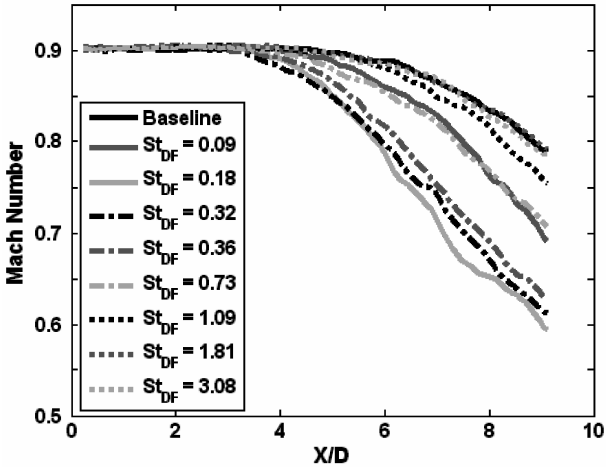

Fig. 8 Jet centerline Mach number distributions for the first helical mode excitation at several forcing St_{DF} ($m = 1$).

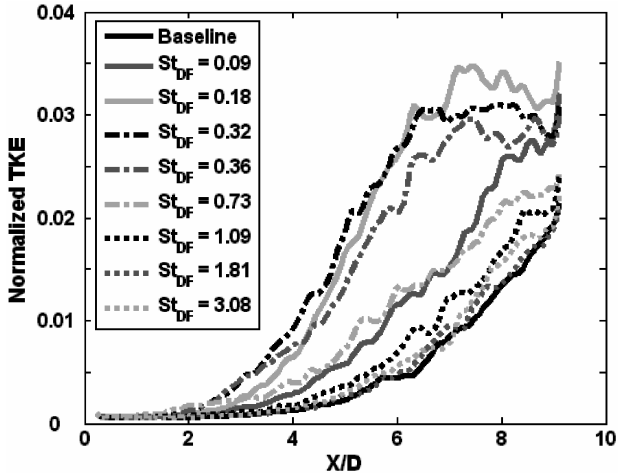

Fig. 10 Centerline turbulent kinetic energy at various forcing St_{DF} for $m = 1$ mode.

about 0.013. Emission spectroscopy-based temperature measurements show an approximate average temperature perturbation of 1000 to 2000°C, depending upon the excitation frequency and duty cycle, imposed by an actuator at the actuation location [48]. This high-amplitude forcing could be a possible reason for the jet not responding to the excitation at (or close to) the jet most amplified Strouhal number. Although not shown here, the trends are similar when forcing at azimuthal modes $m = 0$ and ± 1, with the changes less dramatic for the former and more dramatic for the latter cases, in comparison with the results shown in Fig. 8.

Figure 9 shows the effects of forcing of the jet with various azimuthal modes at a Strouhal number of 0.32. The results show that forcing the jet at all of the modes from $m = 0$ to $m = \pm 4$ affects the jet to varying degrees, in agreement with the flow visualization and perturbation development results (Figs. 5b and 6a). The results are also in agreement with the instability and experimental results in the literature, which have shown that for a thin incoming boundary layer ($D/\theta \sim 250$ in the present case) the jet responds to all lower azimuthal mode disturbances [10,11]. The axisymmetric ($m = 0$) and higher-order modes ($m = 3$ and ± 4) forcing are the least, and the lower mixed modes ($m = \pm 1$ and ± 2) are the most effective, in terms of mixing enhancement. As was also mentioned earlier, one has to be cautious in comparing the effects solely based on the centerline decay, because not all of the azimuthal modes are axisymmetric in the average sense, and such a comparison could be misleading.

Figure 10 shows normalized centerline turbulent kinetic energy (TKE) $[(\sigma_u^2 + \sigma_v^2)/U_J^2]$ for the baseline jet and excited jet with $m = 1$ and various St_{DF}. The trends are very similar to the centerline Mach

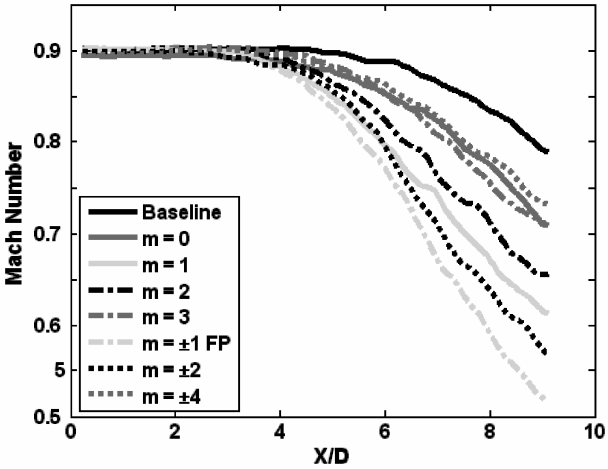

Fig. 9 Centerline Mach number distributions for several forcing modes at $St_{DF} = 0.32$.

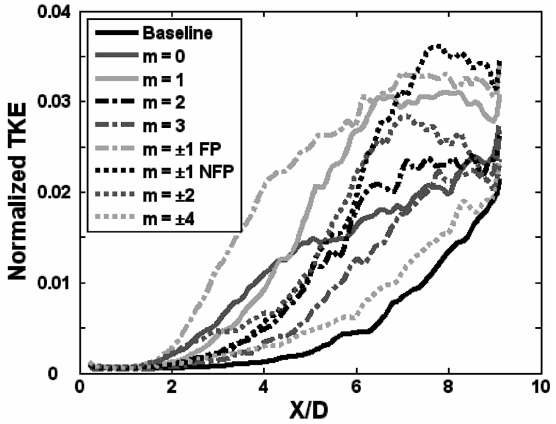

Fig. 11 Centerline turbulent kinetic energy for various forcing modes at $St_{DF} = 0.32$.

number results shown in Fig. 8. The dramatic increase in TKE around the jet's preferred-mode Strouhal number is consistent with the centerline Mach number results shown in Fig. 8, development of perturbation/instability waves in Fig. 5, and are the results of entrainment and gross mixing by larger-scale coherent structures observed in the flow visualization images.

Figure 11 shows normalized centerline turbulent kinetic energy for the baseline jet and the jet forced at $St_{DF} = 0.32$ with various azimuthal modes. The trends are, to some degree, similar to the ones shown for the centerline Mach number, except that the $m = 0$ mode forcing effect, which is quite strong earlier, is reduced significantly farther downstream. The effects of forcing the jet with the $m = 0$ and $m = 1$ modes are very similar to the results of perturbation/instability development in Fig. 5b. Although turbulent kinetic energy for some excitation modes approaches the baseline value by the last measurement location ($x/D \sim 9$), for some others ($m = \pm 1$ and 1) it still remains quite higher, again in agreement with the results in Fig. 5b.

D. Far-Field Acoustic Results

Far-field acoustic results were obtained mostly at two angles with respect to the jet axis: 30 and 90 deg. The results presented here are for the Mach 0.9 jet and all have been normalized to a radius of $80D$. Figure 12 depicts far-field power spectra for the jet forced close to the jet-preferred mode ($St_{DF} = 0.36$) at two different azimuthal modes of $m = 0$ and 3. The first noticeable feature on these spectra is the appearance of the forcing tone and its harmonics. In the axisymmetric azimuthal mode ($m = 0$) forcing case, the forcing

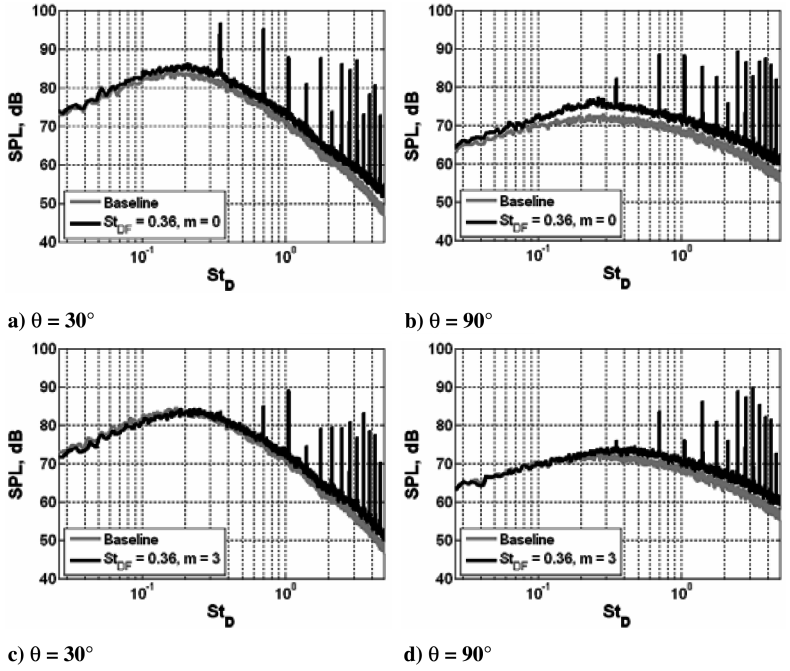

Fig. 12 Far-field acoustic power spectra at 30 and 90 deg for excitation around jet-preferred Strouhal number ($St_{DF} = 0.36$) with two different azimuthal modes ($m = 0$ and 3).

frequency appears in the spectra at both 30- and 90-deg locations, but is more prominent at 30 deg than at 90 deg. However, in exciting the third helical mode ($m = 3$), the forcing tone is barely noticeable at either the 30- or 90-deg spectra. It is known that helical modes do not radiate to the far field as effectively as the axisymmetric mode [43]. Comparison of these results with the results from a recent preliminary work using a jet with an approximately 7.5 times larger exit diameter nozzle showed similar actuation tone amplitude in both the smaller and the larger jets [59]. Because noise intensity scales with nozzle diameter squared, contributions of actuation tones become much smaller in larger nozzles used in practical cases.

Exciting the jet at this low Strouhal number with the $m = 0$ mode (Figs. 12a and 12b), the far-field noise is increased over the entire Strouhal number range, but more at 90 deg than at 30 deg, in agreement with the results in the literature (in which acoustic drivers were used for the excitation) [3,36–38]. Forcing the jet at $m = 3$ mode (Figs. 12c and 12d), far-field noise is still increased at 90 deg, but not over the entire Strouhal number range (only beyond about the forcing Strouhal number) and not as much as the $m = 0$ case. In addition, there is now a slight noise reduction at 30 deg at lower St_{DF} and a smaller noise increase beyond the forcing Strouhal number. The switchover Strouhal number (the Strouhal number above which noise is increased) keeps increasing when the excitation mode is increased from $m = 0$ to 3.

Figure 13 shows far-field acoustic results at a much higher forcing Strouhal number ($St_{DF} = 1.07$) for azimuthal modes 0 and 3. Now,

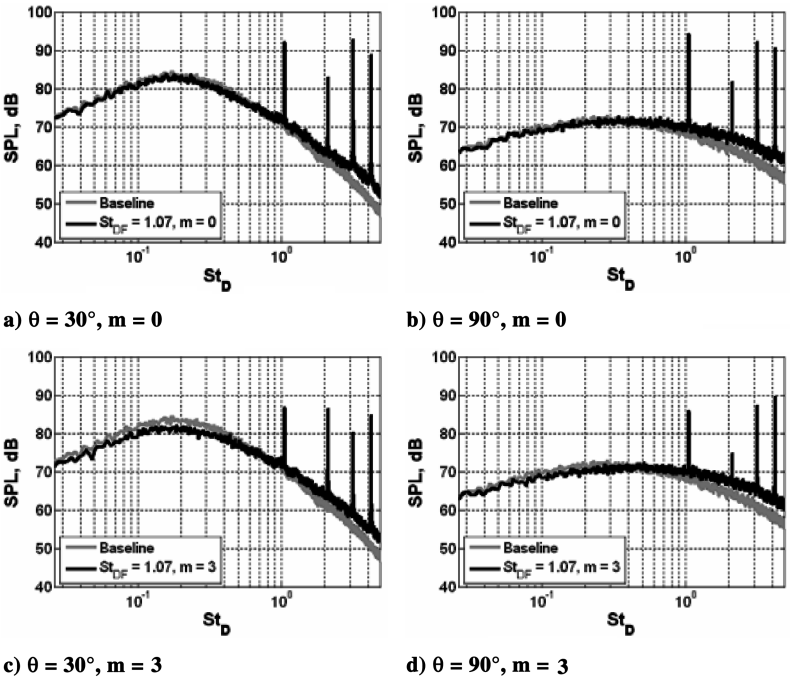

Fig. 13 Far-field acoustic power spectra at 30 and 90 deg for forcing at higher Strouhal number ($St_{DF} = 1.07$) with two different azimuthal mode excitations ($m = 0$ and 3).

even at the axisymmetric mode excitation, there is a slight decrease in noise at both 30 and 90 deg, with the switchover Strouhal number at about the forcing Strouhal number at 30 deg and at a somewhat lower Strouhal number at 90 deg. When excitation at the higher mode ($m = 3$) is used, there is a significant noise reduction at lower Strouhal numbers at 30 deg, with the switchover at the forcing Strouhal number. The trend is the same at 90 deg, but the noise reduction is not as pronounced. These results are consistent with some recent modeling work [60]. These results are again consistent with the seeded perturbation/instability wave development and turbulence results presented and discussed earlier. Dynamics of large-scale and smaller-scale structures are largely responsible for the far-field radiation at 30 and 90 deg, respectively. The results in Fig. 5 show that axisymmetric waves/structures at lower Strouhal numbers grow slowly, stay saturated longer, and decay slowly, resulting in dynamic interaction of large-scale structures for an extensive period of time; hence, there is increased radiated noise at both the 30- and 90-deg directions. On the other hand, instability waves/structures with a higher Strouhal number and higher mode grow faster to lower amplitude and decay faster; hence, there is reduced radiated noise at 30 deg (and to some degree at 90 deg) at lower Strouhal numbers but increased noise at higher Strouhal numbers.

To assess the effect of excitation on broadband noise, the forcing tone and its harmonics are removed during data postprocessing, as it has been done in the literature [3,37]. The rationale for removing the tones for the evaluation is twofold.

1) Because the tones are very narrowband, their contributions to OASPL or any other similar far-field noise measure would be small.

2) They probably would not be present or their contributions would not be significant in large-scale/practical applications. In fact, our preliminary results from larger-scale experiments at NASA seem to support this notion [59].

Figure 14 shows the results presented in Figs. 13c and 13d, but without the tones associated with the excitation. The overall sound pressure level using these spectra can now be calculated for the forced cases. Figure 15 presents the change in the OASPL over the Strouhal number range used in Figs. 12–14 (St_D of 0.01 and 5.0), for both 30- and 90-deg angles, for excitation at various azimuthal modes. Several observations can be made:

1) There is a significant noise increase (2 to 4 dB) when the jet is excited around the jet-preferred instability Strouhal number ($St_{DF} = 0.2$–0.5), which becomes larger from the shallower angle of the jet axis (30 deg) to the larger angle (90 deg). This is in agreement with the results in the literature (in which acoustic drivers were used) [3,36–38].

2) Noise reduction of 0.6 to over 1.0 dB is achieved over a large range of excitation Strouhal numbers. This reduction seems to peak between $St_{DF} = 1.5$ to 2.0 at a 30-deg angle, but at around $St_{DF} = 3.0$ to 3.5 at a 90-deg angle. Similarly, the crossover forcing Strouhal number (from noise increase to noise reduction) is between $St_{DF} = 0.6$ and 1.0 at a 30-deg angle, but around $St_{DF} = 2.0$ at a 90-deg angle.

3) Although the role of azimuthal modes is clear at a 30-deg angle (less noise increase at higher modes, especially at lower forcing Strouhal numbers), the effect is not as clear at higher forcing Strouhal numbers and at a 90-deg angle. There seems to be a clear advantage of excitation of the third helical mode, the highest simple azimuthal mode that could be used with the eight actuators of the current setup, over a large Strouhal number range at a 30-deg-angle location. Future work will include more actuators, enabling forcing at higher helical modes than $m = 3$.

Based on the results already presented and discussed, one could speculate on how the excitation would affect the noise sources within the jet and, in turn, the OASPL at 30- and 90-deg angles. The noise radiated to 30 deg originates mostly from the jet centerline near the end of potential core [58,61], and this is a location at which azimuthal interactions are prevalent [58]. When exciting the jet at a low St_{DF} and low azimuthal modes, the development (the growth, saturation, and decay) of the large-scale structures/instability waves occurs over a large x/D (Figs. 5a, 5b, and 6a). The presence of robust large-scale structures over a large period of time allows prolonged and more vigorous azimuthal interactions. Because of these interactions, the jet then has a shorter potential core (Figs. 8 and 9) and increased TKE (Figs. 10 and 11) along the centerline. These results are consistent with the increase in the far-field OASPL at 30 deg (Figs. 15a and 15c). For excitation at higher St_{DF} and/or higher azimuthal modes, the flowfield pressure showed earlier saturation and faster decay of the instability waves (Figs. 5c, 5d, and 6b), whereas the PIV results showed only slight changes in the potential core length (Figs. 8 and 9) and centerline TKE (Figs. 10 and 11). These results are also consistent with the reduction in the far-field OASPL at 30 deg at higher St_{DF} for all modes and only slightly increase at low St_{DF} for the higher azimuthal modes (Figs. 15a and 15c), implying less rigor during the azimuthal interactions.

It is more difficult to draw any reasonable connection between the flow and far-field results at a 90-deg angle, because the noise at this angle is mostly from dynamics of smaller-scale structures in the jet and the change in OASPL is not very sensitive to azimuthal modes. At this location, most of the noise originates closer to the nozzle exit before any azimuthal interactions have taken place, thus reducing the significance of the azimuthal mode excitation. This is supported by the PIV measurements in which the mean velocity does not begin to decay until at least four jet diameters downstream (Figs. 8 and 9), and the TKE does not begin to increase until after two jet diameters downstream (Figs. 10 and 11). Thus, for the first few jet diameters, the centerline measurements are not dependent on the azimuthal modes. Also, the role of azimuthal mode is not as significant during the initial growth of the structures, as shown in the flowfield pressure results (Figs. 5 and 6). Instead, the initial growth is dependent on the excitation Strouhal number (Figs. 4–6). For the lower Strouhal number, the growth is more gradual, providing a larger noise-source volume, and could be related to the

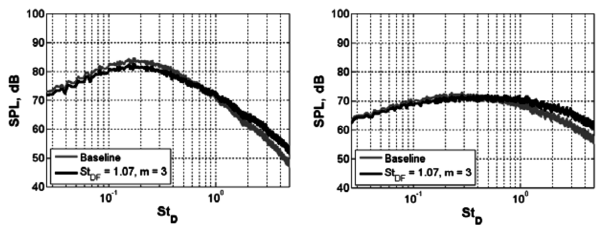

a) θ=30° b) θ=90°

Fig. 14 Far-field acoustic power spectra without the excitation tones at 30 and 90 deg for forcing at $St_{DF} = 1.07$ and $m = 3$.

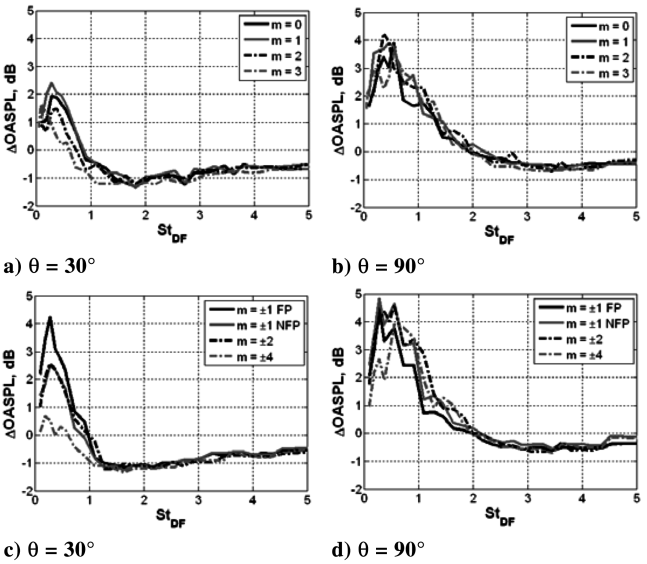

a) θ = 30° b) θ = 90°

c) θ = 30° d) θ = 90°

Fig. 15 Changes in the overall far-field sound pressure level between $St_D = 0.01$ and 4.0 over a large forcing Strouhal number range for different azimuthal modes: a) 30 deg, b) 90 deg, c) 30 deg, and d) 90 deg.

increased OASPL. Although at larger Strouhal numbers, the growth is over a shorter distance, providing a smaller source volume and lower OASPL.

IV. Conclusions

This work is part of an ongoing research in the control of high-speed, high Reynolds number jets for noise mitigation and mixing enhancement. In this work, localized arc filament plasma actuators were used to control an axisymmetric Mach 0.9 jet with a Reynolds number based on the nozzle exit diameter of 7.6×10^5. Eight actuators distributed azimuthally inside the nozzle, approximately 1 mm upstream of the nozzle exit, were used to excite various azimuthal modes of the jet over a large Strouhal number range (St_{DF} of 0.1 to 5.0), which covers the jet-preferred mode and the jet's initial shear layer instability Strouhal number. Real-time pressure measurements within the jet (along a lip line of the nozzle) were used to investigate the growth and decay of seeded perturbations/instability waves in the flow. PIV measurements were used to evaluate the effects of control on the turbulence field, and far-field sound was measured to evaluate the effects of control on the radiated noise field. The jet responded to the forcing over a large range of excitation Strouhal numbers. The development of seeded perturbations by the actuators and instability waves was found to be similar to the reported results in the literature using other techniques such as excitation using acoustic drivers. Excitations with lower Strouhal numbers coupled to the flow, and the instability waves grew slowly, saturated farther downstream, and stayed saturated for a longer time before gradual decay, as expected. The location for the saturation and decay of instability waves moved farther upstream as the excitation Strouhal number was increased. Instability waves with higher azimuthal modes exhibited faster saturation and decay.

Far-field acoustic results were obtained at two angles with respect to the jet axis: 30 and 90 deg. The results were normalized to a radius of $80D$. They show a significant noise increase (2 to 4 dB) when the jet is excited around the jet's preferred-mode instability Strouhal number ($St_{DF} = 0.2$–0.5). The noise amplification becomes larger from the shallower angle of the jet axis (30 deg) to the larger angle (90 deg), in agreement with the results in the literature (in which acoustic drivers were used). Noise reduction of 0.6 to over 1.0 dB is observed over a large range of excitation Strouhal numbers; the reduction seems to peak around $St_{DF} = 1.5$ to 2.0 at a 30-deg angle, but around $St_{DF} = 3.0$ to 3.5 at a 90-deg angle. Although the role of azimuthal modes is clear at a 30-deg angle (less noise increase at higher modes, especially at lower forcing Strouhal numbers), the effect is not as clear at higher forcing Strouhal numbers and at a 90-deg angle. These trends are attributed to the fact that we are controlling large-scale structures in the flow, the dynamics of which are responsible for most of the far-field radiation at 30 deg.

These preliminary results are very encouraging and show the potential of the technique for noise mitigation. However, a great deal more work must be done to better understand the effects and to improve the technique. The current setup with eight actuators limited the azimuthal mode excitation to $m = 3$. The setup will be modified to allow the use of excitation at higher azimuthal modes in the near future.

The power consumption for the eight actuators was less than 1% of the jet flow power and is expected to decrease in larger jets, because the consumed power would increase linearly with the jet diameter D, whereas the jet power would increase with D^2. These actuators with large amplitude and bandwidth (0 to 200 kHz) have opened up tremendous opportunities for control of high-speed, high Reynolds number flows for various purposes (e.g., mixing enhancement and noise mitigation in jets, suppression of cavity tones, and mixing enhancement in combustors).

Acknowledgments

The support of this research by NASA John H. Glenn Research Center and by the Ohio Department of Development is greatly appreciated. The many fruitful discussions with James Bridges and Clifford Brown are greatly appreciated.

References

[1] Brown, G. L., and Roshko, A., "On Density Effects and Large Structure in Turbulent Mixing Layers," *Journal of Fluid Mechanics*, Vol. 64, No. 4, 1974, pp. 715–816.

[2] Winant, C. D., and Browand, F. K., "Vortex Pairing: The mechanism of Turbulent Mixing-Layer Growth at Moderate Reynolds Number," *Journal of Fluid Mechanics*, Vol. 63, No. 2, 1974, pp. 237–252.

[3] Moore, C. J., "The Role of Shear-Layer Instability Waves in Jet Exhaust Noise," *Journal of Fluid Mechanics*, Vol. 80, No. 2, 1977, pp. 321–367.

[4] Ho, C.-M., and Huerre, P., "Perturbed Free Shear Layers," *Annual Review of Fluid Mechanics*, Vol. 16, 1984, pp. 365–424.

[5] Tam, C., "Jet Noise: Since 1952," *Theoretical and Computational Fluid Dynamics*, Vol. 10, Nos. 1–4, 1998, pp. 393–405.

[6] Michalke, A., "On Spatially Growing Disturbances in an Inviscid Shear Layer," *Journal of Fluid Mechanics*, Vol. 23, No. 3, 1965, pp. 521–544.

[7] Michalke, A., "Instability of Compressible Circular Free Jet with Consideration of the Influence of the Jet Boundary Layer Thickness," NASA TM 75190, 1977.

[8] Ho, C.-M., and Huang, L.-S., "Subharmonics and Vortex Merging in Mixing Layers," *Journal of Fluid Mechanics*, Vol. 119, 1982, pp. 443–473.

[9] Plaschko, P., "Helical Instabilities of Slowly Divergent Jets," *Journal of Fluid Mechanics*, Vol. 92, No. 2, 1979, pp. 209–215.

[10] Cohen, J., and Wygnanski, I., "The Evolution of Instabilities in the Axisymmetric Jet, Part 1: The Linear Growth of Disturbances Near the Nozzle," *Journal of Fluid Mechanics*, Vol. 176, 1987, pp. 191–219.

[11] Corke, T. C., Shakib, F., and Nagib, H. M., "Mode Selection and Resonant Phase Locking in Unstable Axisymmetric Jets," *Journal of Fluid Mechanics*, Vol. 223, 1991, pp. 253–311.

[12] Corke, T. C., and Kusek, S. M., "Resonance in Axisymmetric Jets with Controlled Helical-Mode Input," *Journal of Fluid Mechanics*, Vol. 249, 1993, pp. 307–336.

[13] Crow, S., and Champagne, F., "Orderly Structure in Jet Turbulence," *Journal of Fluid Mechanics*, Vol. 48, No. 3, 1971, pp. 547–591.

[14] Zaman, K. B. M. Q., and Hussain, A. K. M. F., "Vortex Pairing in a Circular Jet Under Controlled Excitation, Part 1: General Jet Response," *Journal of Fluid Mechanics*, Vol. 101, No. 3, 1980, pp. 449–491.

[15] Reynolds, W. C., and Bouchard, E. E., "The Effect of Forcing on the Mixing-Layer Region of a Round Jet," *Unsteady Shear Flows*, Springer, New York, 1981, pp. 402–411.

[16] Hussain, A. K. M. F., and Zaman, K. B. M. Q., "The 'Preferred Mode' of the Axisymmetric Jet," *Journal of Fluid Mechanics*, Vol. 110, 1981, pp. 39–71.

[17] Gutmark, E., and Ho, C.-M., "Preferred Modes and the Spreading Rates of Jets," *Physics of Fluids*, Vol. 26, Oct. 1983, pp. 2932–2938.

[18] Crighton, D. G., and Gaster, M., "Stability of Slowly Diverging Jet Flow," *Journal of Fluid Mechanics*, Vol. 77, No. 2, 1976, pp. 387–413.

[19] McMichael, M., "Progress and Prospective for Active Flow Control Using Microfabricated Electromechanical Systems (MEMS)," AIAA Paper 96-0306, Jan. 1996.

[20] Stanek, M., "Control of High Speed Turbulent Free Shear Flows—Stabilization and Destabilization," *International Conference on Computational and Experimental Engineering and Sciences*, 2005.

[21] Samimy, M., Debiasi, M., Caraballo, E., Serrani, A., Yuan, X., Little, J., and Myatt, J., "Feedback Control of Subsonic Cavity Flows Using Reduced-Order Models," *Journal of Fluid Mechanics* (to be published).

[22] Samimy, M., Zaman, K. B. M. Q., and Reeder, M. F., "Effect of Tabs on the Flow and Noise Field of an Axisymmetric Jet," *AIAA Journal*, Vol. 31, No. 4, 1993, p. 609.

[23] Zaman, K. B., Reeder, M. F., and Samimy, M., "Control of an Axisymmetric Jet Using Vortex Generators," *Physics of Fluids*, Vol. 6, No. 2, 1994, pp. 778–793.

[24] Gliebe, P. R., Brausch, J. F., Majjigi, R. K., and Lee, R., "Jet Noise Suppression," *Aeroacoustics of Flight Vehicles: Theory and Practice*, Vol. 2, edited by H. H. Hubbard, NASA, Hampton, VA, 1994, pp. 207–269.

[25] Zaman, K. B. M. Q., "Spreading Characteristics of Compressible Jets from Nozzles of Various Geometries," *Journal of Fluid Mechanics*, Vol. 383, Mar. 1999, pp. 197–228.

[26] Mengle, V. G., "Optimization of Lobe Mixer Geometry and Nozzle Length for Minimum Jet Noise," AIAA Paper 2000-1963, May 2000.

[27] Saiyed, N. H., Mikkelsen, K. L., and Bridges, J. E., "Acoustics and Thrust of Quiet Separate-Flow High-Bypass-Ratio Nozzles," *AIAA Journal*, Vol. 41, No. 3, 2003, pp. 372–378.
[28] Callender, B., and Gutmark, E., "Far-Field Acoustic Investigation into Chevron Nozzle Mechanisms and Trends," *AIAA Journal*, Vol. 43, No. 1, 2005, pp. 87–95.
[29] Tam, C., and Zaman, K. B. M. Q., "Subsonic Jet Noise from Nonaxisymmetric and Tabbed Nozzles," *AIAA Journal*, Vol. 38, No. 4, 2000, pp. 592–599.
[30] Simonich, J., Narayanan, S., Barber, T. J., and Nishimura, M., "Aeroacoustic Characterization, Noise Reduction and Dimensional Scaling Effects of High Subsonic Jets," *AIAA Journal*, Vol. 39, 2001, pp. 2062–2069.
[31] Hileman, J., and Samimy, M., "Turbulence Structures and the Acoustic Far-Field of a Mach 1.3 Jet," *AIAA Journal*, Vol. 39, 2001, pp. 1716–1727.
[32] Arakeri, V. H., Krothapalli, A., Siddavaram, V., Alkislar, M. B., and Lourenco, L. M., "On the Use of Microjets to Suppress Turbulence in a Mach 0.9 Axisymmetric Jet," *Journal of Fluid Mechanics*, Vol. 490, Sept. 2003, pp. 75–98.
[33] Krothapali, A., Venkatakrishnan, L., Lourenco, L., Greska, B., and Elavarasan, R., "Turbulence and Noise Suppression of a High-Speed Jet by Water Injection," *Journal of Fluid Mechanics*, Vol. 491, Sept. 2003, pp. 131–159.
[34] Henderson, B., Kinzie, K., Whitmire, J., and Abeysinghe, A., "The Impact of Fluidic Chevrons on Jet Noise," AIAA Paper 2005-2888, May 2005.
[35] Kibens, V., "Discrete Noise Spectrum Generated by an Acoustically Excited Jet," *AIAA Journal*, Vol. 18, No. 4, 1980, pp. 434–451.
[36] Jubelin, B., "New Experimental Studies on Jet Noise Amplification," AIAA Paper 80-0961, Jan. 1980.
[37] Ahuja, K. K., and Blakney, D. F., "Tone Excited Jets, Part 4: Acoustic Measurements," *Journal of Sound and Vibration*, Vol. 102, No. 1, 1985, pp. 93–117.
[38] Lu, H. Y., "Effect of Excitation on Coaxial Jet Noise," *AIAA Journal*, Vol. 21, No. 2, 1983, pp. 214–220.
[39] Lepicovsky, J., and Brown, W. H., "Effects of Nozzle-Exit Boundary-Layer Conditions on Excitability of Heated Free Jets," AIAA Paper 87-2723, 1987.
[40] Kibens, V., Dorris III, J., and Smith, D. M., "Active Flow Control Technology Transition: The Boeing ACE Program," AIAA Paper 99-3507, 1999.
[41] Morrison, G., and McLaughlin, D., "Noise Generation by Instabilities in Low Reynolds Number Supersonic Jets," *Journal of Sound and Vibration*, Vol. 65, July 1979, pp. 177–191.
[42] Stromberg, J., McLaughlin, D., and Troutt, T., "Flow Field and Acoustic Properties of a Mach Number 0.9 Jet at a Low Reynolds Number," *Journal of Sound and Vibration*, Vol. 72, Sept. 1980, pp. 159–176.
[43] Ginevsky, A. S., Vlasov, Y. V., and Karavosov, R. K., *Acoustic Control of Turbulent Jets*, Springer–Verlag, Berlin, 2004.
[44] Samimy, M., Adamovich, I., Webb, B., Kastner, J., Hileman, J., Keshav, S., and Palm, P., "Development and Characterization of Plasma Actuators for High Speed Jet Control," *Experiments in Fluids*, Vol. 37, No. 4, 2004, pp. 577–588.
[45] Samimy, M., Kim, J.-H., Adamovich, I., Utkin, Y., and Keshav, S., "High Speed Jet Control Using Plasma Actuators," *4th International Symposium on Turbulence and Shear Flow Phenomena*, 2005.
[46] Samimy, M., Kim, J.-H., Adamovich, I., Utkin, Y., and Kastner, J., "Active Control of High Speed and High Reynolds Number Free Jet Using Plasma Actuators," AIAA Paper 2006-0711, Jan. 2006.
[47] Samimy, M., Kim, J.-H., Kastner, J., Adamovich, I., and Utkin, Y., "Active Control of High Speed and High Reynolds Number Jets Using Plasma Actuators," *Journal of Fluid Mechanics* (to be published).
[48] Utkin, Y. G., Keshav, S., Kim, J.-H., Kastner, J., Adamovich, I. V., and Samimy, M., "Development and Use of Localized Arc Filament Plasma Actuators For High-Speed Flow Control," *Journal of Physics D: Applied Physics* (to be published).
[49] Roth, J. R., "Aerodynamic Flow Acceleration Using Paraelectric and Peristaltic Electrohydrodynamic Effects of a One Atmosphere Uniform Glow Discharge Plasma," *Physics of Plasmas*, Vol. 10, No. 5, 2003, pp. 2117–2126.
[50] Post, M. L., and Corke, T. C., "Separation Control on High Angle of Attack Airfoil Using Plasma Actuators," *AIAA Journal*, Vol. 42, No. 11, 2004, pp. 2177–2184.
[51] Henoch, C., and Stace, J., "Experimental Investigation of a Salt Water Turbulent Boundary Layer Modified by an Applied Streamwise Magnetohydrodynamic Body Force," *Physics of Fluids*, Vol. 7, No. 6, June 1995, pp. 1371–1383.
[52] Meyer, R., Nishihara, M., Hicks, A., Chintala, N., Cundy, M., Lempert, W. R., Adamovich, I. V., and Gogineni, S., "Measurements of Flow Conductivity and Density Fluctuations in Supersonic Nonequilibrium MHD Flows," *AIAA Journal*, Vol. 43, No. 9, 2005, pp. 1923–1930.
[53] Bedin, A. P., and Mishin, G. I., "Ballistic Studies of the Aerodynamic Drag on a Sphere in Ionized Air," *Technical Physics Letters*, Vol. 21, 1995, pp. 5–7.
[54] Merriman, S., Plönjes, E., Palm, P., and Adamovich, I. V., "Shock Wave Control by Nonequilibrium Plasmas in Cold Supersonic Gas Flows," *AIAA Journal*, Vol. 39, No. 8, 2001, pp. 1547–1552.
[55] Leonov, S., Bityurin, V., Savelkin, K., and Yarantsev, D., "Effect of Electrical Discharge on Separation Processes and Shocks Position in Supersonic Airflow," AIAA Paper 2002-0355, Jan. 2002.
[56] Tret'yakov, P. K., Garanin, A. F., Grachev, G. N., Krainev, V. L., Ponomarenko, A. G., Tischenko, V. N., and Yakovlev, V. I., "Control of Supersonic Flow Around Bodies by Means of High-Power Recurrent Optical Breakdown," *Physics-Doklady*, Vol. 41, No. 11, 1996, p. 566.
[57] Adelgren, R. G., Yan, H., Elliott, G. S., Knight, D. D., Beutner, T. J., and Zheltovodov, A. A., "Control of Edney IV Interaction by Pulsed Laser Energy Deposition," *AIAA Journal*, Vol. 43, No. 2, 2005, pp. 256–269.
[58] Kastner, J., Hileman, J., and Samimy, M., "Exploring High-Speed Axisymmetric Jet Noise Control Using Hartmann Tube Fluidic Actuators," AIAA Paper 2004-0186, Jan. 2004.
[59] Samimy, M., Kastner, J., Kim, J.-H., Utkin, Y., Adamovich, I., and Brown, C., "Flow and Noise Control in High Speed and High Reynolds Jets Using Plasma Actuators," AIAA Paper 2006-2846, June 2006.
[60] Reba, R., Narayanan, S., and Colonius, T., and Suzuki, T., "Modeling Jet Noise from Organized Structures Using Near-Field Hydrodynamic Pressure," AIAA Paper 2005-3093, May 2005.
[61] Hileman, J., Caraballo, E., Thurow, B., and Samimy, M., "Dynamics of Large-scale Structure and Sound Emission in High-Speed Jets: Real-time Flow Visualization with Simultaneous Acoustic Measurements," *Journal of Fluid Mechanics*, Vol. 544, Dec. 2005, pp. 277–307.

N. Clemens
Associate Editor